Light-Addressable Potentiometric Sensors for Quantitative Spatial Imaging of Chemical Species

Tatsuo Yoshinobu,[1,2] Ko-ichiro Miyamoto,[2] Carl Frederik Werner,[2] Arshak Poghossian,[3,4] Torsten Wagner,[3,4] and Michael J. Schöning[3,4]

[1]Department of Biomedical Engineering, Tohoku University, Sendai 980–8579, Japan; email: nov@ecei.tohoku.ac.jp

[2]Department of Electronic Engineering, Tohoku University, Sendai 980–8579, Japan

[3]Institute of Nano- and Biotechnologies, Aachen University of Applied Sciences, Jülich Campus, Jülich 52428, Germany

[4]Peter Grünberg Institute, Research Centre Jülich GmbH, Jülich 52425, Germany

Annu. Rev. Anal. Chem. 2017. 10:225–46

First published as a Review in Advance on March 27, 2017

The *Annual Review of Analytical Chemistry* is online at anchem.annualreviews.org

https://doi.org/10.1146/annurev-anchem-061516-045158

Keywords

LAPS, chemical imaging sensor, pH sensor, biosensor, bioimaging

Abstract

A light-addressable potentiometric sensor (LAPS) is a semiconductor-based chemical sensor, in which a measurement site on the sensing surface is defined by illumination. This light addressability can be applied to visualize the spatial distribution of pH or the concentration of a specific chemical species, with potential applications in the fields of chemistry, materials science, biology, and medicine. In this review, the features of this chemical imaging sensor technology are compared with those of other technologies. Instrumentation, principles of operation, and various measurement modes of chemical imaging sensor systems are described. The review discusses and summarizes state-of-the-art technologies, especially with regard to the spatial resolution and measurement speed; for example, a high spatial resolution in a submicron range and a readout speed in the range of several tens of thousands of pixels per second have been achieved with the LAPS. The possibility of combining this technology with microfluidic devices and other potential future developments are discussed.

1. INTRODUCTION

A light-addressable potentiometric sensor (LAPS) (1–5) is a semiconductor-based chemical sensor that was proposed by Hafeman et al. (1) in 1988. The typical structure of a LAPS sensor plate and a measurement setup are schematically illustrated in **Figure 1**. It belongs to the family of field-effect sensors that have an electrolyte-insulator-semiconductor (EIS) structure (6–10), in which the sensing surface of the insulating layer is in contact with the solution to be analyzed. An ion-sensitive field-effect transistor (ISFET) (11–14) and an EIS capacitive sensor (15–20) are two other examples of chemical sensors belonging to the same family.

These sensors detect redistribution of carriers inside the semiconductor layer caused by variation of the potential on the sensing surface responding to the analyte concentration. Whereas an ISFET detects variation of the source–drain conductance, an EIS capacitive sensor and a LAPS detect variation of the capacitance of the depletion layer in the semiconductor, the thickness of which responds to the analyte concentration on the sensing surface. In a LAPS, the variation of the capacitance is read out in the form of an AC photocurrent signal induced by illumination, whereas the capacitance in an EIS capacitive sensor is electrically measured.

As indicated by its name, a LAPS is capable of spatially resolved measurement through the use of a localized illumination. This light addressability implies further applications of the LAPS in three different ways. First, a multiwell sensor device (1, 21–24) can be realized by defining a plurality of measurement sites on a single sensor plate, each of which functions as an independent sensor for the same species. Second, a multianalyte sensor device (1, 25–30) can be achieved by depositing different sensing membranes on a plurality of measurement sites, each of which is sensitive to different species. Third, a LAPS can be applied to chemical imaging (30, 31), in which the spatial distribution of a particular species is visualized. This type of sensor was initially

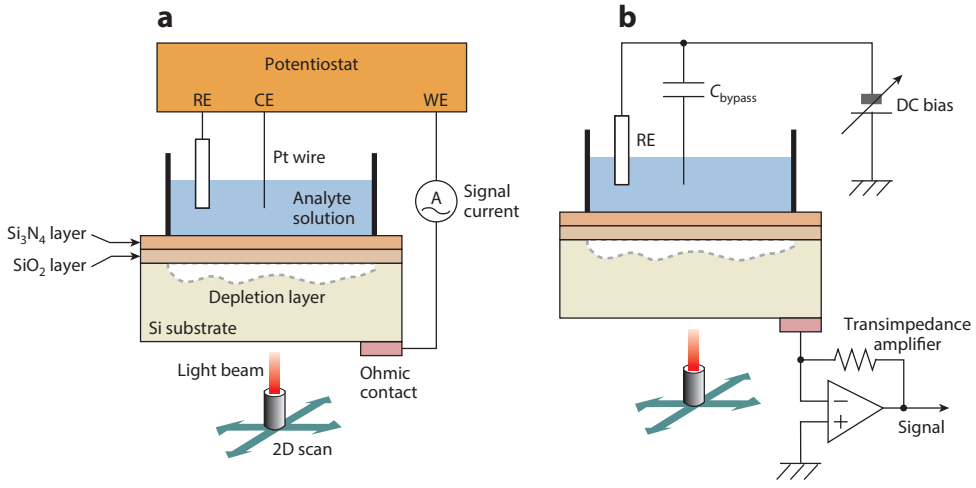

Figure 1

(*a*) A typical layer structure of a light-addressable potentiometric sensor plate and a standard three-electrode configuration. A DC bias is applied between the RE and the semiconductor substrate. An AC photocurrent signal is generated by illuminating the semiconductor substrate with a modulated light beam and measured by an AC ammeter (A). (*b*) A simplified setup using a bypass capacitor. The semiconductor substrate is virtually grounded via a transimpedance amplifier, which converts the photocurrent signal into a voltage signal. Abbreviations: 2D, two-dimensional; CE, counter electrode; Pt, platinum; RE, reference electrode; WE, working electrode.

called a pH-imaging sensor, as it was first employed to visualize a pH distribution (32–34). A more generalized term, chemical imaging sensor (35), was introduced later to refer to sensors that visualize the distribution of other chemical species as well. This review summarizes and discusses the state-of-the-art technologies of chemical imaging sensor systems based on LAPS.

2. FEATURES OF THE LIGHT-ADDRESSABLE POTENTIOMETRIC SENSOR

Visualization of analyte distribution is an essential technology in many disciplines of science, laboratory analysis, and industrial processes. Applications include analysis of chemical and electrochemical reactions, investigation of biological samples such as organs, tissues, and cells, the study of material surfaces, and inspection of food samples. For such purposes, there exists a variety of technologies, including (*a*) various staining methods (36) combined with fluorescence microscopy, (*b*) scanning electrochemical microscopy (SECM) (37), and (*c*) arrayed electrodes/sensors, such as microelectrode arrays (38–41), ISFET arrays (42–45), charge-coupled device-based chemical imaging sensors (46–50), and a field-effect–addressable potentiometric sensor/stimulator (51). Staining methods are widely used and especially preferred in biology and medicine, thanks to the variety of available dyes and the maturity of optical imaging technologies. SECM probes a surface with a microelectrode tip and provides information on electrochemical kinetics at a high spatial resolution. Arrayed electrodes/sensors rely on microfabrication technologies, which integrate a large number of measurement sites on a single chip at a high density. Direct wirings and peripheral circuits allow fast readout from individual electrodes/sensors.

In comparison, a LAPS-based chemical imaging sensor has the following features. The variety of measurable species and the detection limit are essentially the same as those of other potentiometric sensors, such as an ISFET. The spatial resolution is typically on the order of 10 to 100 μm, but possibilities of submicron resolution have been also reported (52–54). In contrast to arrayed electrodes/sensors, a LAPS sensor plate has no built-in pixel structures, and the pixel layout is defined by a scanning light beam at the time of use. The absence of built-in pixel structures in a LAPS sensor plate has the following advantages. First, the pixel layout can be flexibly changed for zooming in and out. There is no limitation in the number of pixels, and the measurement area can be as large as desired with any shape. Second, there is no need for wires connecting pixels and passivation to protect wires from the solution, which makes it durable for long-term use. Third, the flatness of the sensing surface makes it easy to combine a LAPS with microfluidics. Finally, a LAPS sensor plate requires no microfabrication processes such as photolithography, which makes it low cost and applicable to disposable uses.

3. MEASUREMENT SYSTEM

A chemical imaging sensor system consists of a LAPS sensor plate, a light source, and optics with a scanning mechanism to deliver a light beam to different locations on the sensor plate; it also comprises an electrochemical setup, measurement electronics, and software. The front side of a semiconductor plate is covered with an insulating layer, whose surface serves as the sensing surface. The semiconductor plate is typically made of Si with a resistivity in the range of 1 to 10 Ω and a thickness of 100–200 μm, covered with stacked layers of SiO_2 and Si_3N_4, with a total thickness of approximately 100 nm. Although the sensor signal is an AC photocurrent, a LAPS is a potentiometric sensor, in which the potential on the sensing surface responds to the analyte concentration. The mechanism in which the surface potential responds to the analyte concentration is essentially the same as in an ISFET and is explained by the

SCANNED LIGHT-PULSE TECHNIQUE

A measurement setup similar to that of a LAPS-based chemical imaging sensor system was originally employed in the scanned light–pulse technique (SLPT) (142) for visualization of interface properties, such as the flat-band voltage and the concentration of interface states in a metal-insulator–semiconductor system. A measurement setup without a metal layer was also proposed (92), in which distributions of crystal defects and interface trap densities in a thermally oxidized Si wafer were visualized by collecting the current through a capacitively coupled electrode placed near the oxide surface via an air gap, instead of directly contacting the oxide surface. SLPT was also applied to gas sensing by using a catalytic metal layer deposited on the insulator surface (143–146). An artificial olfactory image (143), a two-dimensional response pattern obtained with a combination of catalytic metals with a temperature gradient, was proposed as a fingerprint of gases. As an application of an olfactory image, diagnosis of diabetes based on the olfactory image of the breath was proposed (146).

site-dissociation–site-binding model (8, 55–58). Materials such as Si_3N_4 (1), Al_2O_3 (59, 60), Ta_2O_5 (61), HfO_2 (62, 63), and NbO_x (64) have been used for pH sensing. An SiO_2 interlayer is often inserted to lower the density of surface states at the insulator–semiconductor interface. An anodic oxide (54) and a self-assembled organic monolayer (65) exhibit higher sensitivities. Various chemical species other than H^+ can be also selectively measured by modifying the sensing surface with appropriate sensing materials. See sidebar, Scanned Light-Pulse Technique, for details of the method, which employs a similar measurement setup.

An ohmic contact is formed on the back side of the sensor plate to read out the AC photocurrent signal as well as to apply a DC bias voltage across the EIS system. A standard setup constitutes a three-electrode system that consists of a reference electrode (RE) such as Ag/AgCl, a counter electrode such as platinum wire, and a sensor plate as a working electrode (WE) (**Figure 1*a***). Because no DC current flows through the EIS system, a potentiostat can be omitted by using a bypass capacitor (**Figure 1*b***). In the literature, two different notations are used to describe the bias voltage, following different conventions of electrochemistry and semiconductor electronics, respectively; a bias voltage refers to the potential of the semiconductor substrate (i.e., WE) with respect to the RE in electrochemistry and vice versa in semiconductor electronics, in which the Si substrate is considered as a reference.

A modulated light, typically in the form of periodic pulses in a frequency range of 100 Hz to 100 kHz (66–68), illuminates the sensor plate to generate an AC photocurrent signal. In the case of an Si sensor plate, either visible or near-infrared light with a photon energy larger than the bandgap is used. For spatially resolved measurements, a focused light beam scans the sensor plate to obtain a photocurrent map, which is converted into a chemical image. Two different arrangements, frontside and backside illuminations, are possible (66, 69, 70). Whereas backside illumination requires diffusion of photocarriers across the sensor plate, frontside illumination generates photocarriers directly inside the depletion layer, which is advantageous in terms of a larger current signal, a higher cutoff frequency, and a higher spatial resolution. In the case of frontside illumination, however, scattering and absorption of light by the specimen placed on the sensing surface disturb uniform delivery of light (71); therefore, a backside illumination is more often used.

In a typical setup, a laser beam is focused onto the backside of the sensor plate through an objective lens, and the light spot is moved by means of a mechanical scan stage (25, 35, 72) or mirrors (32, 73) for raster scanning of the area to be measured. In some setups, an arrayed light source, such as a light-emitting diode (LED) array (70, 74) and a vertical-cavity surface-emitting

laser array (75), are employed for parallel readout from a plurality of locations on the sensing surface. A pixel of a display panel (76) or video projector (77, 78) can be also employed as a light source. On one hand, these light sources are advantageous in terms of miniaturization, as they require no mechanical scan, but on the other hand, the flexibility of the pixel layout is limited.

The AC photocurrent signal of the WE is converted by a transimpedance amplifier into a voltage signal, which is digitally sampled and processed (72) to generate a chemical image. The AC photocurrent is typically in the range of 10 nA to 1 μA, and the gain of the transimpedance amplifier is selected in the range of 10^5 to 10^7 V/A. A field-programmable gate array is advantageous for real-time data processing (79).

4. PRINCIPLES OF OPERATION AND MODELING

Generation of an AC photocurrent signal in a LAPS is understood as follows (66, 80). When the light is turned on, photocarriers, i.e., pairs of electrons and holes, are generated by absorption of photons in the semiconductor layer. Although a certain part of photocarriers is lost by recombination, electrons and holes arriving at the depletion layer by diffusion are separated by the electric field inside the depletion layer, resulting in a transient current. When the light is turned off, excess electrons and holes eventually recombine, resulting in a transient current in the opposite direction. The analyte concentration can be determined by measuring the current, as it depends on the capacitance of the depletion layer.

Figure 2*a* depicts a circuit model, in which repeated generation of a transient current by modulated illumination is represented by an AC current source, I_{photo}, to be divided by the capacitance of the insulating layer, C_i, and the capacitance of the depletion layer, C_d, in the illuminated area (81, 82). Z_s is the serial impedance of the external circuit including the solution, the electrochemical double layer on the sensing surface, the semiconductor layer, the backside contact, and the input impedance of the transimpedance amplifier. The variable g_d is the conductance across the depletion layer due to photocarriers. If both Z_s and g_d are negligibly small, the AC photocurrent

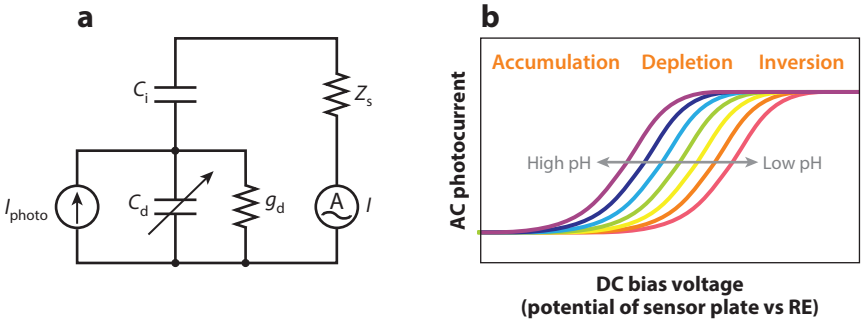

Figure 2

(*a*) A circuit model of a LAPS, in which repeated generation of photocarriers by a modulated light beam is represented by an AC current source I_{photo} to be divided by C_d, C_i, and g_d connected to Z_s. C_d is the capacitance of the depletion layer that responds to the analyte concentration, C_i is the capacitance of the insulating layers, g_d is the conductance of the depletion layer, and Z_s is the serial impedance of the external circuit. The AC photocurrent signal, I, is measured by an ammeter (A). (*b*) A schematic of AC photocurrent–DC bias voltage (*I–V*) curves of a LAPS sensor plate that shift along the voltage axis with a Nernstian response. An example of pH response of a LAPS sensor plate with an n-type semiconductor is shown. Abbreviations: LAPS, light-addressable potentiometric sensor; RE, reference electrode.

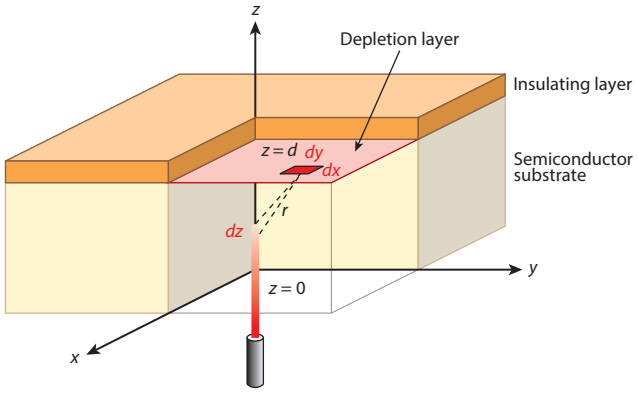

Figure 3

A schematic representation of a carrier diffusion model in the case of backside illumination. The incident light beam enters the semiconductor substrate and generates electron–hole pairs (photocarriers) at a different depth from the back surface. The loss of photocarriers in the course of diffusion toward the front side is characterized by the diffusion length of minority carriers. Photocarriers that arrive at the depletion layer contribute to the current signal depending on the local value of C_d/C_i (34). The illuminated point on the back surface of the semiconductor substrate is the origin of the *xyz* coordinate system, in which z is the depth from the back surface and d is the thickness of the semiconductor substrate. Abbreviations: C_d, capacitance of the depletion layer; C_i, capacitance of the insulating layer.

signal I is given by a simple expression,

$$I = I_{\text{photo}} \cdot \frac{C_i}{C_i + C_d}, \qquad 1.$$

where C_d varies with the bias voltage across the EIS system.

Figure 2*b* shows an example of current–voltage (I–V) characteristics of a LAPS with n-type Si for different pH values. For a fixed pH value, I increases as the EIS system is more depleted and C_d is reduced. The surface potential responds to pH according to the Nernst equation, resulting in a shift of the (I–V) curve along the voltage axis.

To investigate the operation of a chemical imaging sensor, a carrier diffusion model (33, 34, 66, 69, 83) for the case of backside illumination, schematically shown in **Figure 3**, has been employed. In this model, the AC photocurrent signal is calculated as follows. First, the number of electron–hole pairs generated at a depth between z and $z + dz$ from the back surface in a unit of time is given by

$$\frac{P}{h\nu} \cdot \alpha \cdot \exp(-\alpha z) \cdot dz, \qquad 2.$$

where P is the power of the incident light beam, $h\nu$ is the photon energy, and α is the absorption coefficient of light in the semiconductor. Second, by assuming isotropic diffusion of carriers and taking account of recombination in the course of diffusion, the number of minority carriers arriving at an infinitesimal area $dxdy$ of the depletion layer in a unit of time is given by

$$\int_{z=0}^{d} \left[\frac{P}{h\nu}\alpha \cdot \exp(-\alpha z) \cdot dz \cdot \exp\left(-\frac{r}{L}\right) \cdot \frac{dxdy}{4\pi r^2} \cdot \frac{d-z}{r} \right] \qquad 3.$$

$$= \frac{\alpha P}{4\pi h\nu} \left[\int_{z=0}^{d} \exp\left(-\alpha z - \frac{r}{L}\right) \cdot \frac{d-z}{r^3} \cdot dz \right] dxdy,$$

where d is the thickness of the semiconductor layer, L is the diffusion length of minority carriers, and r is the traveling distance of minority carriers given by

$$r = \sqrt{x^2 + y^2 + (d - z)^2}\ . \qquad 4.$$

Finally, the total AC photocurrent signal I is calculated by integrating the contribution of each area on the sensing surface, taking account of the local value of C_d/C_i, which varies with the local concentration of analyte. Using the carrier diffusion model, the dependence of the signal intensity, and the spatial resolution of a chemical imaging sensor on various parameters, such as the thickness of the semiconductor layer, the wavelength of the incident light, and the diffusion length of minority carriers have been investigated. A fair agreement between predictions and experimental results has been demonstrated in spite of simplifications (34, 83).

In some cases, however, assumptions of the carrier diffusion model are oversimplifications, and other factors also significantly affect the performance of the chemical imaging sensor. Guo et al. (84) pointed out that an increase of excess carriers reduces the local thickness of the depletion layer, depending on the light intensity and the distance from the illuminated point. Poghossian et al. (85) showed the influence of the capacitive coupling of the solution and semiconductor substrate through the entire LAPS surface in contact with the solution. This coupling acts as an AC current path in parallel to the external circuit, as shown in **Figure 4**. If the impedance of the capacitive coupling is small and comparable to that of the external circuit Z_s, which may occur at higher frequencies and for a large contact area, the AC photocurrent signal measured in the external circuit is reduced, depending on both the local value and the global distribution of analyte concentration.

A physical simulation based on a semiconductor device simulator (68, 84, 86) allows a much more detailed analysis of the operation of a chemical imaging sensor. It takes into account the generation, drift, diffusion, and recombination of electrons and holes in a semiconductor and numerically calculates the temporal changes of distributions of the potential and carrier

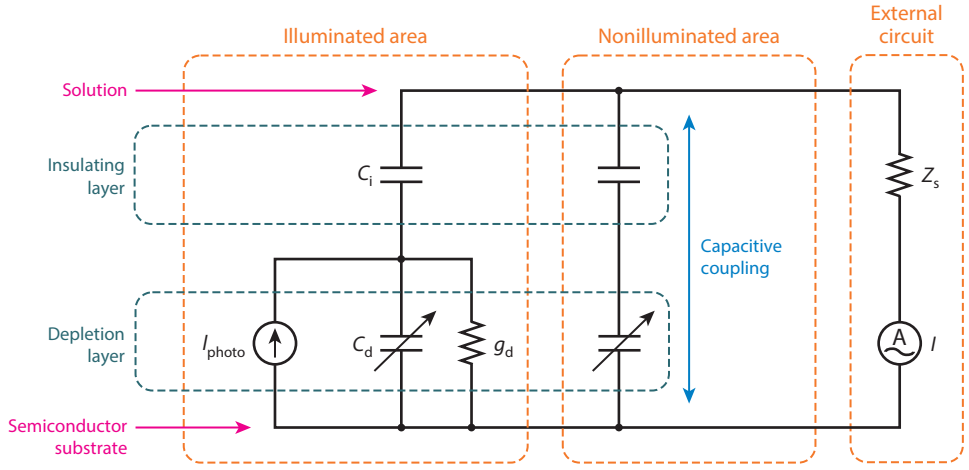

Figure 4

An additional current path due to capacitive coupling of the solution and the semiconductor substrate through the insulating layer and the depletion layer of the nonilluminated area. When the impedance of the capacitive coupling is comparably small to the serial impedance of the external circuit Z_s, the current signal to be measured in the external circuit is reduced. Adapted with permission from Reference 85. Copyright 2017, Elsevier. Abbreviations: C_d, capacitance of the depletion layer; C_i, capacitance of the insulating layer; g_d, conductance across the depletion layer due to photocarriers.

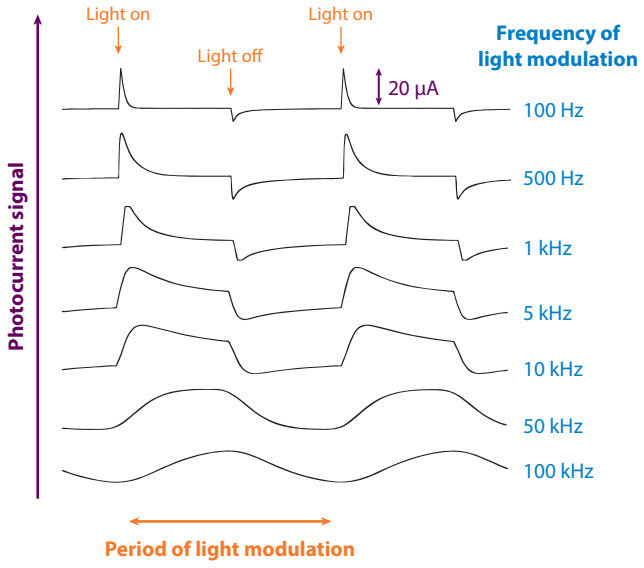

Figure 5

AC photocurrent signals reproduced in a physical simulation of a light-addressable potentiometric sensor (LAPS) operation by a semiconductor device simulator. In the simulation, a light beam with a wavelength of 700 nm modulated at different frequencies of 100 Hz–100 kHz illuminated a 200-μm-thick LAPS sensor plate, and the subsequent generation, diffusion, drift, and recombination of photocarriers were numerically calculated. Adapted with permission from Reference 68. Copyright 2014, John Wiley & Sons.

concentrations. The effects of various parameters, such as the wavelength, intensity, and modulation frequency of light, the lifetime of minority carriers, and the thickness of the semiconductor substrate and insulating layers, can be investigated. **Figure 5** shows an example of simulated waveforms of the AC photocurrent signal at different frequencies, which were in good agreement with experimental results. An extension of a semiconductor device simulator that includes the analyte solution was recently proposed for an ISFET (87). This would provide even more detailed and accurate information on the performance of a chemical imaging sensor, considering the distribution of double-layer capacitance, impedance of the solution, the geometry of electrodes, and the capacitive coupling between the solution and the semiconductor substrate.

5. MEASUREMENT MODES

When the potential of the LAPS surface varies in response to the analyte concentration, the effective DC bias applied to the EIS system varies accordingly. This change can be quantified by measuring the horizontal displacement of the *I–V* curve represented by the bias voltage corresponding to the inflection point of the curve, either by numerically calculating the second derivative (1, 88) or by fitting the curve with a model function (89). The horizontal location of the inflection point can then be correlated to the analyte concentration through the calibration step. As explained in the sidebar, Scanning Photo-Induced Impedence Microscopy, the variation of the vertical height of the *I–V* curve is detected for impedance mapping.

In imaging applications, however, it is usually too time consuming to acquire the *I–V* curves at all pixels. In the constant-bias mode (32), which is the most frequently used measurement mode of a chemical imaging sensor, the DC bias is fixed at a constant value within the transition part

SCANNING PHOTO-INDUCED IMPEDANCE MICROSCOPY

Whereas a variation of the analyte concentration results in a horizontal shift of the *I–V* curve of a LAPS sensor plate along the voltage axis, the serial impedance of the analyte affects the vertical height of the *I–V* curve. The spatial distribution of the impedance within a specimen can therefore be visualized by recording the AC photocurrent at a constant bias voltage fixed in the inversion region, where the current is no longer dependent on the bias voltage. This measurement mode is called scanning photo–induced impedance microscopy (SPIM) (147). The measurement setup and procedure of the SPIM mode are exactly the same as those of the constant-bias mode LAPS except that the bias voltage is set in the inversion region in the former and in the depletion region in the latter. A submicron resolution was achieved by the two-photon effect (54, 65), and high-resolution SPIM was applied to the visualization of impedance change in PAH/PSS polyelectrolyte microcapsules labeled with Au nanoparticles (148).

of the *I–V* curve, where a map of the AC photocurrent signal is acquired. The photocurrent map is then converted into a map of potential shift using the average slope of the transition part of the *I–V* curve and then converted further into a map of the analyte concentration. An essential limitation of the constant-bias mode is that the measurable range of the potential shift is limited within the transition part of the *I–V* curve. When it is necessary to measure a large variation of analyte concentration, the constant-current mode (90) or the potential-tracking mode (89) is used.

In the constant-current mode (90), a feedback loop controls the DC bias to maintain the AC photocurrent signal at a constant value, and the required offset of the DC bias is recorded, which is then converted into the variation of analyte concentration. If the initial value of the AC photocurrent signal is spatially uniform, a common target value can be set for all pixels, which is not usually the case. In a general case, the initial values of the AC photocurrent signal are recorded at all pixels within the first scan. During the subsequent scans, a feedback loop controls the DC bias to reproduce the initial value of the AC photocurrent signal at each pixel.

In the potential-tracking mode (89), the horizontal shift of the *I–V* curve at each pixel is detected. Instead of measuring the *I–V* curve at each pixel, a series of AC photocurrent maps is acquired at several DC bias voltages, from which the *I–V* curves are reconstructed at all pixels. Although the total number of data is the same, the latter scheme is much faster because the DC bias is scanned only once throughout the measurement. Every time the DC bias is updated, a settling time is required until the capacitance of the entire sensing surface in contact with the solution is charged at the new DC bias. The number of bias voltages at which the AC photocurrent maps are acquired can be relatively small, and a sparse set of data points on the *I–V* curve at each pixel is fitted to a model function, such as a logistic function to calculate the horizontal shift. The potential-tracking mode can follow a large displacement of the *I–V* curve, and it is robust against variation of the height of the *I–V* curve, which is caused by variation of the impedance of the solution.

Whereas the conventional measurement modes rely on variation of the amplitude of an AC photocurrent signal in response to the analyte concentration, the phase shift of an AC photocurrent signal with respect to the excitation light can be correlated to the analyte concentration (91). The advantage of the phase mode over the conventional amplitude mode is that the phase of the AC photocurrent is much less sensitive to certain types of disturbances that affect the amplitude. The crystal defects in Si are known to result in nonuniformity of the carrier recombination rate (92). Although an amplitude image is strongly affected by the distribution of defects, a phase image is immune to it (91).

Table 1 Target species of a light-addressable potentiometric sensor other than H^+ reported in the literature

Type of target species	Target species	Type of sensing element	Reference(s)
Cations	K^+, Mg^{2+}, Ca^{2+}	Ionophore/PVC membrane	59
	Na^+, K^+, Ca^{2+}	Ionophore/PVC membrane	27
	Li^+, K^+, Ca^{2+}	Ionophore/PVC membrane	28, 29
	Li^+, K^+, Cs^+, Mg^{2+}, Ca^{2+}	Ionophore/photocurable membrane	30, 93
	Pb^{2+}	Chalcogenide glass	96
	Fe^{3+}, Pb^{2+}, Cr^{6+}	Chalcogenide glass	94
	Cd^{2+}	Chalcogenide glass	95
	Na^+	Oxide (CF_4 plasma-treated HfO_2)	62
	NH_4^+	Oxide (CF_4 plasma-treated HfO_2)	63
Anions	F^-	Ionic crystal (LaF_3)	97
	NO_3^-	Organic ion exchanger/PVC membrane	98
	SO_4^{2-}	Ionophore/PVC membrane	
	Cl^-	Oxide (nitrogen-incorporated Sm_2O_3)	99
Molecules	Ethanol	Enzyme (in solution)	100
	Urea, glucose	Enzyme	26
	Urea	Enzyme	35, 103
	Urea, penicillin, glucose	Enzyme	101
	Acetylcholine (chloride, iodide), butyrylthiocholine (iodide)	Enzyme	105
	Penicillin	Enzyme	7, 104
	Urea, butyrylcholine (iodide)	Enzyme	102
	Acetylcholine (chloride)	Enzyme	106
	ATP	ATP-sensitive aptamer	108
	ssDNA	Complimentary ssDNA immobilized on graphene oxide	109
	ssDNA	Complimentary ssDNA immobilized on SiO_2	110–112
Taste substances	NaCl, HCl, quinine, saccharose, sodium glutamate monohydrate	Artificial lipid membranes	25

Abbreviations: ATP, adenosine triphosphate; PVC, polyvinyl chloride; ssDNA, single-stranded DNA.

6. TARGET SPECIES

In addition to measurement of pH or the activity of H^+, the LAPS surface can also be functionalized to respond to a variety of other chemical species. As members of the family of potentiometric sensors, many technologies that have been developed for ion-selective electrodes, ISFETs, and EIS capacitive sensors are also applicable to functionalization of a LAPS surface. **Table 1** summarizes various target species of a LAPS that were thus far reported in the literature.

Several different types of sensing elements have been employed to produce an ion-sensitive LAPS. For example, sensitivities to the alkali metal ions Na^+ (27), Li^+ (29, 30, 93), K^+ (27–30, 59, 93), and Cs^+ (30, 93) and the alkaline earth metal ions Mg^{2+} (30, 59, 93) and Ca^{2+} (27, 28, 30, 59, 93) have been achieved with corresponding ionophores in a liquid membrane supported by polyvinyl chloride or a photocurable membrane. Several heavy metal ions, such as Cr^{6+} (94), Fe^{3+}, (94), Cd^{2+} (95), and Pb^{2+} (94, 96), were detected by a chalcogenide glass membrane deposited

on a LAPS surface using a pulsed-laser deposition technique. Sensors for several anions [F^- (97), NO_3^- (98), and SO_4^{2-} (98)] have been realized with different types of sensing elements on a LAPS surface. Enhancement of cross sensitivities of an oxide surface to ions other than H^+ have been also reported (62, 63, 99).

Another large category of functionalization relies on the biocatalytic activity of enzyme molecules immobilized on a LAPS surface. Examples of enzymes applied to a LAPS include alcohol dehydrogenase (100), urease (26, 35, 101–103), penicillinase (7, 101, 104), glucose oxidase (26, 101), acetylcholinesterase (105, 106), and butyrylcholinesterase (102, 105). In some cases, a substrate-rich condition was employed to quantify the enzyme concentration rather than the substrate concentration (100). Toxins were detected by measuring the inhibition rate of an enzymatic activity (102, 105, 107). Various types of sandwich immunoassays for proteins, viruses, and bacteria, as well as a gene probe assay and an inhibition assay, were demonstrated with a LAPS measuring the enzymatic activity of urease conjugated to an antifluorescein antibody binding to a fluoresceinated antibody (107).

Yet another category of functionalization relies on the specific binding or affinity of molecules. A LAPS surface functionalized with an adenosine triphosphate (ATP)-sensitive aptamer monitored ATP secreted by a taste receptor cell (108). Detection of a potential change caused by hybridization of a single-stranded DNA (ssDNA) and a complementary probe ssDNA on a LAPS surface was also reported (109–112). In a multianalyte application, a set of artificial lipid membranes was prepared by a modified Langmuir-Blodgett method, and their responses to taste substances were investigated (25).

7. CALIBRATION

Similar to all chemical sensors, a LAPS requires calibration at a certain frequency depending on the accuracy needed. In a calibration procedure, *I–V* curves are acquired for several standard solutions of known concentrations, and their inflection points are determined. The slope sensitivity is then obtained by least-square fitting the plot of bias voltages at inflection points as a function of the logarithm of analyte concentration.

In the case of imaging, additional procedures are necessary to correct for in-plane nonuniformities inherent to an individual sensor plate. Two types of nonuniformities in a sensor plate are known (113). The first type originates from the distribution of defects in the semiconductor crystal, at which the current signal is reduced due to a loss of carriers by enhanced recombination (92, 114). The second type of nonuniformity arises from contamination of the sensing surface, such as the intake of ions into the insulating layer during use, which changes the local flat-band voltage of the EIS system. These two types of nonuniformities can be corrected for by using a pair of calibration maps, i.e., a current calibration map and a potential calibration map, prepared for the particular sensor plate through the measurement of a homogeneous solution (113).

8. SPATIAL RESOLUTION

Spatial resolution is one of the most important indices representing the performance of a chemical imaging sensor, as it determines the smallest structure that can be observed. Because a LAPS sensor plate has no isolations between neighboring pixels, spatial resolution is determined by the lateral extent to which photocarriers diffuse in the semiconductor layer (31, 66, 83).

In a case where a light illuminates a point on the back side of a sensor plate, and the thickness of the semiconductor layer d is much larger than the penetration depth of the light, the photocarriers diffuse three-dimensionally from the illuminated point (**Figure 6*a***). In a simplified model,

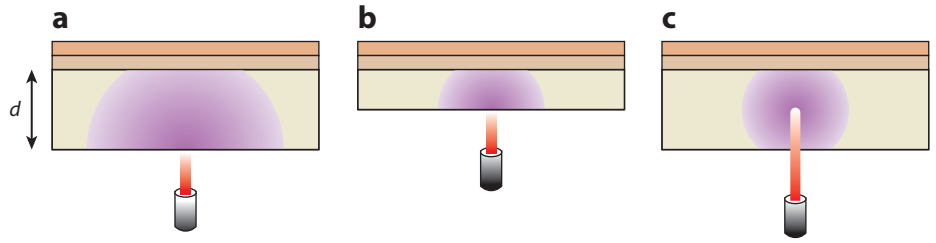

Figure 6

Schematic illustrations of (*a*) the diffusion of photocarriers from the illuminated point on the backside of a light-addressable potentiometric sensor (LAPS) plate, (*b*) the effect of thinning the sensor plate, and (*c*) the effect of using an infrared light that enters deeper into the sensor plate. The thickness of the sensor plate is denoted by *d* and the arrow.

the spatial resolution in this case is given by $\sqrt{L \cdot (L + 2d)}$, where L is the diffusion length of minority carriers (31). In a case of the other extreme, where d is small, the carrier diffusion is two-dimensional, and the spatial resolution is given by L.

The simplest approach to improve the spatial resolution is reducing the thickness of the semiconductor layer d (33, 66, 69, 83) (**Figure 6*b***). However, a sensor plate thinner than 100 μm is fragile, and some mechanical support is indispensable for a practical application. A 5-μm test pattern was resolved with a LAPS sensor plate based on a silicon-on-sapphire (SOS) wafer with an active layer of 0.5 μm (115).

The use of an infrared light, which generates photocarriers after entering deeper into Si, has an effect equivalent to reduction of the thickness of the sensor plate (34) (**Figure 6*c***). A 10-μm test pattern was resolved with a 20-μm Si sensor plate in combination with an infrared light with a wavelength of 830 nm, which had a penetration depth of 13 μm (34).

Another approach to improving spatial resolution is to choose a semiconductor material with a shorter diffusion length L. In the case of a thick substrate, however, a smaller L also means more loss of carriers, which results in a small current signal (66). Therefore, the sensor plate must be thin when a semiconductor material has a smaller L. A spatial resolution of 15 μm was obtained by increasing the doping concentration of Si to reduce L and by thinning the sensor plate (69). Semiconductor materials with a direct bandgap, such as GaAs (116) and GaN (117), have a smaller value of L compared to those with an indirect bandgap, such as Si, and it is expected to achieve a higher resolution. A spatial resolution better than 3.1 μm was obtained for a LAPS sensor plate with an 8-nm epilayer of GaAs (116). A spatial resolution in a submicron range was obtained with a thin-film amorphous Si deposited on a transparent glass substrate (52).

A method based on the two-photon effect, which was previously applied to optical beam–induced current imaging (118), was proposed to enhance spatial resolution (54, 65). An infrared light with a wavelength of 1,250 nm, the photon energy of which was smaller than the energy bandgap of Si, was focused inside the sensor plate, so that photocarriers were generated by the two-photon effect only in the vicinity of the focal point near the depletion layer. With this technique applied to an SOS with an active layer of 0.5 μm, a spatial resolution of 0.8 μm was achieved (54).

An auxiliary illumination to improve the spatial resolution was also devised (119, 120). In this method, a ring-shaped constant light illuminates the surrounding of the modulated light and increases the carrier concentration. Enhanced carrier recombination in the surrounding region blocks the lateral diffusion of photocarriers induced by the modulated light. This effect was predicted by simulation (119) and experimentally verified (120).

Yet another method to improve spatial resolution based on temporal analysis of the transient current signal was recently proposed (121). A short pulse of a laser beam illuminates a point on the sensor plate, from which photocarriers start diffusion. The transient current signal is then recorded at a high temporal resolution. An earlier part of the signal reflects charging of the capacitance near the illuminated point, whereas a later part includes the signal from distant locations. Therefore, the spatial resolution can be improved by reducing the integral time of the transient current signal. The validity of this approach was verified both by simulation and experiments (121).

9. HIGH-SPEED MEASUREMENT

The image acquisition time of a chemical imaging sensor is given by the product of the measurement time per pixel and the number of pixels, so far as a single light beam is used for readout. The measurement time per pixel is chosen to obtain a satisfactory signal-to-noise ratio, if not limited by the speed of mechanical scan. In a typical setup, where the frequency of the modulated light is several kilohertz, and the sampling time is chosen to include several tens of cycles, the typical measurement time per pixel is on the order of milliseconds. Therefore, a typical image acquisition time at a resolution of 128×128 pixels, for example, is on the order of minutes, which would be acceptable for recording slow processes, such as cell growth (122, 123) and corrosion of a metal surface (124). To record faster processes or to enhance the throughput of analysis, however, reduction of the measurement time is indispensable.

The image acquisition time can be greatly reduced by using more than one light beam for readout in parallel (125). In this method, a plurality of light beams modulated at different frequencies illuminates different locations of the sensor plate and generates an AC photocurrent depending on the local analyte concentrations at respective locations. The current signal measured in the external circuit is a superposition of respective frequency components, which can be separated by lock-in detection. For separation of signals in the frequency domain, the frequency step, Δf, must be larger than or at least equal to the inverse of the sampling time, T_s; therefore, a frequency bandwidth of $N_c \times \Delta f \geq N_c/T_s$ is required, where N_c is the number of channels or multiplicity.

This technique based on frequency-division multiplex was applied to a multianalyte sensor (94, 126) and a chemical imaging sensor (70, 74, 127). A chemical imaging sensor system with a multiplicity of $N_c = 64$ was constructed (74), in which 64 locations on the sensing surface were simultaneously illuminated by light beams from 64 LEDs guided by optical fibers and driven at different frequencies between 6.4 and 12.7 kHz with $\Delta f = 100$ Hz. Frequencies below 6.4 kHz were skipped to avoid interference of harmonics. The sampling frequency, the number of samplings, and the sampling time, T_s, were 400 kHz, 4,000, and 10 ms, respectively, which realized a movie recording of pH at a frame rate of 100 frames per second (fps). **Figure 7** shows a series of snapshots extracted from a movie recording, in which a buffering action of phosphate buffer was recorded (74).

The highest frequency that can be used for a LAPS is determined by the low-pass filtering effect of carrier diffusion across the sensor plate (66). The available bandwidth can be therefore extended by using frontside illumination (66, 70) or a thinner sensor plate, which allows modulation of carrier concentrations at higher frequencies. A movie recording at an even higher frame rate would be accomplished by increasing Δf and reducing T_s. For example, a frame rate of 1,000 fps would be achieved for a multiplicity $N_c = 64$ using a set of frequencies between 64 and 127 kHz with $\Delta f = 1$ kHz, which corresponds to a readout speed of 64,000 pixels/s. However, a dramatic increase in the multiplicity N_c seems difficult, considering the available bandwidth and complexity of the light source. Thus, to increase the pixel number in movie recording, a combination of arrayed

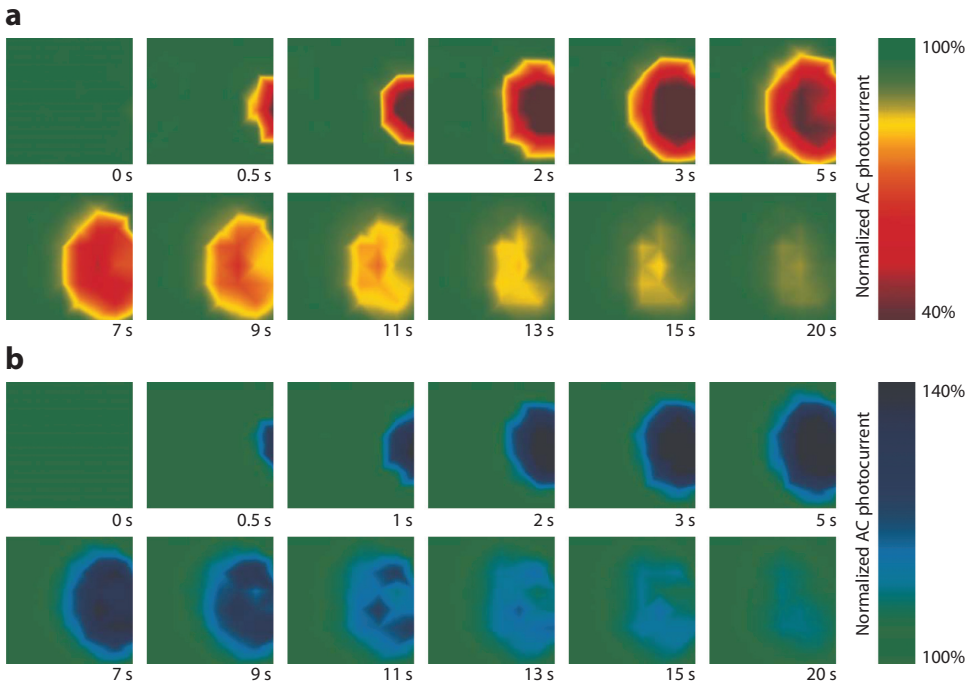

Figure 7

A series of snapshots extracted from a movie recording at 100 frames per second, in which a buffering action of phosphate buffer was recorded. (*a*) Samples of 0.2 ml of 10 mM HCl and (*b*) 0.2 ml of 10 mM NaOH were injected into 2 ml of phosphate buffer, respectively, at a rate of 0.1 ml/s. A temporary change and subsequent recovery of pH were clearly observed. An area of 12×12 mm^2 was illuminated by 8×8 optical fibers delivering 64 light beams modulated at different frequencies in the range of 6.4 to 12.7 kHz with $\Delta f =$ 100 Hz (74).

light beams and a scanning technique seems to be a realistic solution, which makes a compromise between the pixel number and frame rate.

10. APPLICATIONS

Historically, much effort has been directed toward biological and biomedical applications of a LAPS used as a microphysiometer (2, 21, 88, 128–133), which quantifies the response of metabolic activity of cells to chemical substances for the purpose of drug screening. A cell-semiconductor hybrid LAPS (134) was proposed as a cell-based biosensor to detect the response of the extracellular potential to chemical substances.

As an imaging version of LAPS, a chemical imaging sensor was applied, for example, to visualize the pH distributions around microbial colonies cultured on agarose (32, 34, 122). This method is expected to automate the plate count and quantify the metabolic activity of individual colonies. Efforts have been also made to record the extracellular potentials of cardiac myocytes (71) and neural cells (135–137) cultured on a LAPS surface. Recently, application of a LAPS to deep brain imaging was proposed (138). A tiny LAPS chip with a dimension of 500×500 μm^2 was attached to the tip of a flexible polymer-based neural probe, which included conducting wires and optical waveguide bundle for delivering an array of light beams to the LAPS chip for spatially resolved

LIGHT-ADDRESSABLE ELECTRODES FOR ELECTROCHEMISTRY

The insulating layer on the LAPS surface blocks DC current, which allows potentiometric sensing of the surface potential at equilibrium but prohibits electrochemical reactions on the surface. There have been attempts inspired by LAPS to control the localized electrochemical reactions, taking advantage of light addressability. Suzurikawa et al. (149) proposed a light-addressable electrode, in which a low-conductive passivation layer on a-Si:H contacted the solution. The light addressability in this case relied on the photoconductivity of a-Si:H, the illuminated region of which functioned as a current path. An arbitrary shape of region defined by illumination with a digital micromirror device functioned as an anode or a cathode in electrolysis to create a pH gradient in the solution. Choudhury et al. (150) proposed the concept of light-activated electrochemistry, in which a hydrogen-terminated Si surface modified with organic monolayers contacted the solution, and a DC faradaic current was allowed to flow only at an illuminated location with a micron-scale resolution.

measurement. This device could record neuronal activities as well as pH values. The probe was chronically implanted into the hippocampal formation of the brain of a mouse, and the low-frequency brain events were successfully recorded. Other examples of biomedical applications include visualization of pH changes on plant leaves in response to an acidic droplet (139), surface analysis of dentinal caries in human teeth (140), and visualization of the recovery process of a cultured cell layer of human epithelial cells, Caco-2 (123).

The chemical imaging sensor is also useful in the field of materials science. It was recently applied to the study of crevice corrosion of stainless steel. (124). In spite of the high resistance to corrosion, stainless steel is known to corrode when placed in a gap of a few micrometers. Because the gap is narrow and difficult to access for analysis, the mechanism of crevice corrosion is not fully understood. The sensing surface of a LAPS was placed in the proximity of the surface of the test piece with a narrow gap filled with seawater, and the pH change associated with corrosion was successfully visualized under potentiostatic polarization.

Another possible application of a chemical imaging sensor is its use as a readout unit of a microfluidic device, such as a micrototal analysis system or a lab-on-a-chip. By constructing a microfluidic device on the flat sensing surface of a chemical imaging sensor (21), spatiotemporal change of pH or the concentration of a target species inside the microchannel can be visualized (141), which provides useful information to analyze the dynamics of reaction and diffusion. This format is advantageous for analyzing many small-volume samples in parallel, which makes it a prospective strategy to develop new types of high-throughput biomedical assays (31). In addition to sensing and imaging, the light-addressing technique has been applied to induce localized electrochemical reactions (see sidebar, Light-Addressable Electrodes for Electrochemistry).

11. SUMMARY AND OUTLOOK

The performance of LAPS-based chemical imaging sensor systems has been greatly enhanced over the past two decades. Various technologies to improve the spatial resolution were invented, and a high spatial resolution in the submicron range has been achieved. An array of light beams enabled parallel access to a plurality of pixels to acquire a signal multiplexed in the frequency domain for fast readout in the range of several tens of thousands of pixels per second. A number of measurement modes have been devised to meet different requirements and priorities of particular applications. Researchers established a calibration procedure to correct for in-plane nonuniformities of an individual sensor plate.

There seem to be two different strategies for further development of LAPS-based chemical imaging sensor systems. The developments thus far are mainly directed to construct a general-purpose instrument that can be adapted for a wide variety of analyses. This strategy was successful in enhancing the instrument's overall performance. For more practical applications, however, development of a customized instrument would be valuable to elicit high performance to meet specific requirements. More application-oriented development will be key to expanding the usability of LAPS-based chemical imaging sensor systems.

DISCLOSURE STATEMENT

The authors are not aware of any affiliations, memberships, funding, or financial holdings that might be perceived as affecting the objectivity of this review.

LITERATURE CITED

1. LAPS was introduced and proposed as a platform for various assays.

5. An extensive review of LAPS literature as of 2007.

1. **Hafeman DG, Parce JW, McConnell HM. 1988. Light-addressable potentiometric sensor for biochemical systems. *Science* 240:1182–85**
2. McConnell HM, Owicki JC, Parce JW, Miller DL, Baxter GT, et al. 1992. The cytosensor microphysiometer: biological applications of silicon technology. *Science* 257:1906–12
3. Owicki JC, Bousse LJ, Hafeman DG, Kirk GL, Olson JD, et al. 1994. The light-addressable potentiometric sensor: principles and biological applications. *Annu. Rev. Biophys. Biomol. Struct.* 23:87–114
4. Katsube T. 1999. Light addressable potentiometric chemical sensing system. In *Sensors Update* Vol. 6, ed. H Baltes, H, W Göpel, J Hesse, pp. 19–40. Weinheim, Ger.: Wiley-VCH Verlag
5. **Wagner T, Schöning MJ. 2007. Light-addressable potentiometric sensors (LAPS): recent trends and applications. In *Electrochemical Sensor Analysis*, ed. S Alegret, A Merkoçi, pp. 87–128. Amsterdam: Elsevier**
6. Schöning MJ, Poghossian A, Yoshinobu T, Lüth H. 2001. Semiconductor-based field-effect structures for chemical sensing. *Proc. SPIE* 4205:188–98
7. Poghossian A, Yoshinobu T, Simonis A, Ecken H, Lüth H, Schöning MJ. 2001. Penicillin detection by means of field-effect based sensors: EnFET, capacitive EIS sensor or LAPS? *Sens. Actuators B* 78:237–42
8. Vlasov YG, Tarantov YA, Bobrov PV. 2003. Analytical characteristics and sensitivity mechanisms of electrolyte-insulator-semiconductor system-based chemical sensors—a critical review. *Anal. Bioanal. Chem.* 376:788–96
9. Schöning MJ, Poghossian A. 2006. Bio FEDs (field-effect devices): state-of-the-art and new directions. *Electroanalysis* 18:1893–900
10. Bratov A, Abramova N, Ipatov A. 2010. Recent trends in potentiometric sensor arrays—a review. *Anal. Chim. Acta* 678:149–59
11. Bergveld P. 1970. Development of an ion-sensitive solid-state device for neurophysiological measurements. *IEEE Trans. Biomed. Eng.* 17:70–71
12. Esashi M, Matsuo T. 1974. An integrated field-effect electrode for biopotential recording. *IEEE Trans. Biomed. Eng.* 21:485–87
13. Moss SD, Johnson CC, Janata J. 1978. Hydrogen, calcium, and potassium ion-sensitive FET transducers: a preliminary report. *IEEE Trans. Biomed. Eng.* 25:49–54
14. Schöning MJ, Poghossian A. 2002. Recent advances in biologically sensitive field-effect transistors (BioFETs). *Analyst* 127:1137–51
15. Siu WM, Cobbold RSC. 1979. Basic properties of the electrolyte-SiO_2–Si system: physical and theoretical aspects. *IEEE Trans. Electron Devices* 26:1805–15
16. de Rooij NF, Bergveld P. 1980. The influence of the pH on the electrolyte-SiO_2-Si system studied by ion-sensitive FET measurements and quasi-static C-V measurements. *Thin Solid Films* 71:327–31
17. Grattarola M, Cambiaso A, Cenderelli S, Tedesco M. 1989. Capacitive measurements in electrolyte-insulator-semiconductor (EIS) systems modified by biological materials. *Sens. Actuators* 17:451–59

18. Klein M. 1990. Characterization of ion-sensitive layer systems with a *C*(*V*) measurement method operating at constant capacitance. *Sens. Actuators B* 1:354–56
19. Beyer M, Menzel C, Quack R, Scheper T, Schügerl K, et al. 1994. Development and application of a new enzyme sensor type based on the EIS-capacitance structure for bioprocess control. *Biosens. Bioelectron.* 9:17–21
20. Abouzar MH, Poghossian A, Cherstvy AG, Pedraza AM, Ingebrandt S, Schöning MJ. 2012. Label-free electrical detection of DNA by means of field-effect nanoplate capacitors: experiments and modeling. *Phys. Status Solidi A* 209:925–34
21. Baxter GT, Bousse LJ, Dawes TD, Libby JM, Modlin DN, et al. 1994. Microfabrication in silicon microphysiometry. *Clin. Chem.* 40:1800–4
22. Schöning MJ, Wagner T, Wang C, Otto R, Yoshinobu T. 2005. Development of a handheld 16 channel pen-type LAPS for electrochemical sensing. *Sens. Actuators B* 108:808–14
23. Wagner T, Yoshinobu T, Rao C, Otto R, Schöning MJ. 2006. "All-in-one" solid-state device based on a light-addressable potentiometric sensor platform. *Sens. Actuators B* 117:472–79
24. Wagner T, Rao C, Kloock JP, Yoshinobu T, Otto R, Schöning MJ. 2006 "LAPS Card"—a novel chip card-based light-addressable potentiometric sensor (LAPS). *Sens. Actuators B* 118:33–40
25. Kanai Y, Shimizu M, Uchida H, Nakahara H, Zhou CG, Maekawa H, Katsube T. 1994. Integrated taste sensor using surface photovoltage technique. *Sens. Actuators B* 20:175–79
26. Shimizu M, Kanai Y, Uchida H, Katsube T. 1994. Integrated biosensor employing a surface photovoltage technique. *Sens. Actuators B* 20:187–92
27. Wu Y, Wang P, Ye X, Zhang Q, Li R, et al. 2001. A novel microphysiometer based on MLAPS for drugs screening. *Biosens. Bioelectron.* 16:277–86
28. Ermolenko Y, Yoshinobu T, Mourzina Y, Furuichi K, Levichev S, et al. 2003. The double K^+/Ca^{2+} sensor based on laser scanned silicon transducer (LSST) for multi-component analysis. *Talanta* 59:785–95
29. Ermolenko YE, Yoshinobu T, Mourzina YG, Vlasov YG, Schöning MJ, Iwasaki H. 2004. Laser-scanned silicon transducer (LSST) as a multisensor system. *Sens. Actuators B* 103:457–62
30. Yoshinobu T, Iwasaki H, Ui Y, Furuichi K, Ermolenko Y, et al. 2005. The light-addressable potentiometric sensor for multi-ion sensing and imaging. *Methods* 37:94–102
31. Yoshinobu T, Miyamoto K, Wagner T, Schöning MJ. 2015. Recent developments of chemical imaging sensor systems based on the principle of the light-addressable potentiometric sensor. *Sens. Actuators B* 207:926–32
32. Nakao M, Yoshinobu T, Iwasaki H. 1994. Scanning-laser-beam semiconductor pH-imaging sensor. *Sens. Actuators B* 20:119–23
33. Nakao M, Yoshinobu T, Iwasaki H. 1994. Improvement of spatial-resolution of a laser-scanning pH-imaging sensor. *Jpn. J. Appl. Phys.* 33:L394–97
34. Nakao M, Inoue S, Yoshinobu T, Iwasaki H. 1996. High-resolution pH imaging sensor for microscopic observation of microorganisms. *Sens. Actuators B* 34:234–39
35. Inoue S, Nakao M, Yoshinobu T, Iwasaki H. 1996. Chemical-imaging sensor using enzyme. *Sens. Actuators B* 32:23–26
36. Horobin RW, Kernan JA, eds. 2002. *Conn's Biological Stains: A Handbook of Dyes, Stains and Fluorochromes for Use in Biology and Medicine*. Oxford, UK: BIOS Sci. 10th ed.
37. Bard AJ, Fan FRF, Kwak J, Lev O. 1989. Scanning electrochemical microscopy. Introduction and principles. *Anal. Chem.* 61:132–38
38. Meyer H, Drewer H, Gruendig B, Cammann K, Kakerow R, et al. 1995. Two-dimensional imaging of O_2, H_2O_2, and glucose distributions by an array of 400 individually addressable microelectrodes. *Anal. Chem.* 67:1164–70
39. Feeney R, Kounaves SP. 2000. Microfabricated ultramicroelectrode arrays: developments, advances, and applications in environmental analysis. *Electroanalysis* 12:677–84
40. Zoski CG, Simjee N, Guenat O, Koudelka-Hep M. 2004. Addressable microelectrode arrays: characterization by imaging with scanning electrochemical microscopy. *Anal. Chem.* 76:62–72
41. Lin Z, Takahashi Y, Kitagawa Y, Umemura T, Shiku H, Matsue T. 2008. An addressable microelectrode array for electrochemical detection. *Anal. Chem.* 80:6830–33

32. A scanning system was proposed for LAPS-based pH imaging.

42. Bove M, Cambiaso A, Grattarola M, Martinoia S, Verreschi G. 1995. An array of H^+ FETs for space-resolved electrochemical measurements in microenvironments. *Sens. Actuators B* 24:218–21
43. Goh CZD, Georgiou P, Constandinou TG, Prodromakis T, Toumazou C. 2011. A CMOS-based ISFET chemical imager with auto-calibration capability. *IEEE Sens. J.* 11:3253–60
44. Nemeth B, Piechocinski MS, Cumming DRS. 2012. High-resolution real-time ion-camera system using a CMOS-based chemical sensor array for proton imaging. *Sens. Actuators B* 171–2:747–52
45. Shields P, Nemeth B, Green RB, Riehle MO, Cumming DRS. 2012. High-speed imaging of 2-D ionic diffusion using a 16 × 16 pixel CMOS ISFET array on the microfluidic scale. *IEEE Sens. J.* 12:2744–49
46. Sawada K, Mimura S, Tomita K, Nakanishi T, Tanabe H, et al. 1999. Novel CCD-based pH imaging sensor. *IEEE Trans. Electron Devices* 46:1846–49
47. Hattori T, Masaki Y, Atsumi K, Kato R, Sawada K. 2010. Real-time two-dimensional imaging of potassium ion distribution using an ion semiconductor sensor with charged coupled device technology. *Anal. Sci.* 26:1039–45
48. Takenaga S, Tamai Y, Okumura K, Ishida M, Sawada K. 2012. Label-free acetylcholine image sensor based on charge transfer technology for biological phenomenon tracking. *Jpn. J. Appl. Phys.* 51:027001
49. Futagawa M, Suzuki D, Otake R, Dasai F, Ishida M, Sawada K. 2013. Fabrication of a 128 × 128 pixels charge transfer type hydrogen ion image sensor. *IEEE Trans. Electron Devices* 60:2634–39
50. Edo Y, Tamai Y, Yamazaki S, Inoue Y, Kanazawa Y, et al. 2015. 1.3 mega pixels CCD pH imaging sensor with 3.75 μm spatial resolution. *IEEE Int. Electron Devices Meet.* (2105):29.3.1–3.4
51. Parak WJ, George M, Gaub HE, Böhm S, Lorke A. 1999. The field-effect-addressable potentiometric sensor/stimulator (FAPS)—a new concept for a surface potential sensor and stimulator with spatial resolution. *Sens. Actuators B* 58:467–504
52. Moritz W, Yoshinobu T, Finger F, Krause S, Martin-Fernandez M, Schöning MJ. 2004. High resolution LAPS using amorphous silicon as the semiconductor material. *Sens. Actuators B* 103:436–41
53. Zhang Q. 2005. Theoretical analysis and design of submicron-LAPS. *Sens. Actuators B* 105:304–11
54. Chen L, Zhou YL, Jian SH, Kunze J, Schmuki P, Krause S. 2010. High resolution LAPS and SPIM. *Electrochem. Commun.* 12:758–60
55. Yates DE, Levine S, Healy TW. 1974. Site-binding model of the electrical double layer at the oxide/water interface. *J. Chem. Soc. Faraday Trans.* 1 70:1807–18
56. Fung CD, Cheung PW, Ko WH. 1986. A generalized theory of an electrolyte-insulator-semiconductor field-effect transistor. *IEEE Trans. Electron Devices* 33:8–18
57. Bousse L, Meindl JD. 1986. Surface potential-pH characteristics in the theory of the oxide-electrolyte interface. In *ACS Symp. Ser.* Vol. 323, ed. JA Davis, KF Hayes, pp. 79–98. Washington, DC: Am. Chem. Soc.
58. van Hal REG, Eijkel JCT, Bergveld P. 1996. A general model to describe the electrostatic potential at electrolyte oxide interface. *Adv. Colloid Interface Sci.* 69:31–62
59. Seki A, Motoya K, Watanabe S, Kubo I. 1999. Novel sensors for potassium, calcium and magnesium ions based on a silicon transducer as a light-addressable potentiometric sensor. *Anal. Chim. Acta* 382:131–36
60. Ismail ABM, Harada T, Yoshinobu T, Iwasaki H, Schöning MJ, Lüth H. 2000. Investigation of pulsed laser-deposited Al_2O_3 as a high pH-sensitive layer for LAPS-based biosensing applications. *Sens. Actuators B* 71:169–72
61. Yoshinobu T, Ecken H, Poghossian A, Lüth H, Iwasaki H, Schöning MJ. 2001. Alternative sensor materials for light-addressable potentiometric sensors. *Sens. Actuators B* 76:388–92
62. Lue CE, Lai CS, Chen HY, Yang CM. 2010. Light addressable potentiometric sensor with fluorine-terminated hafnium oxide layer for sodium detection. *Jpn. J. Appl. Phys.* 49:04DL05
63. Yang JH, Lu TF Wang JC, Yang CM, Pijanowska DG, Chin CH, et al. 2013. LAPS with nanoscaled and highly polarized HfO_2 by CF_4 plasma for NH_4^+ detection. *Sens. Actuators B* 180:71–76
64. Yang CM, Chiang TW, Yeh YT, Das A, Lin YT, Chen TC. 2015. Sensing and pH-imaging properties of niobium oxide prepared by rapid thermal annealing for electrolyte-insulator-semiconductor structure and light-addressable potentiometric sensor. *Sens. Actuators B* 207:858–64

52. Submicron resolution was obtained with amorphous Si LAPS.

54. Submicron resolution was obtained using the two-photon effect.

65. Wang J, Zhou Y, Watkinson M, Gautrot J, Krause S. 2015. High-sensitivity light-addressable potentiometric sensors using silicon on sapphire functionalized with self-assembled organic monolayers. *Sens. Actuators B* 209:230–36
66. Sartore M, Adami M, Nicolini C, Bousse L, Mostarshed S, Hafeman D. 1992. Minority-carrier diffusion length effects on light-addressable potentiometric sensor (LAPS) devices. *Sens. Actuators A* 32:431–36
67. Werner CF, Wagner T, Yoshinobu T, Keusgen M, Schöning MJ. 2013. Frequency behaviour of light-addressable potentiometric sensors. *Phys. Status Solidi A* 210:884–91
68. Guo Y, Miyamoto K, Wagner T, Schöning MJ, Yoshinobu T. 2014. Theoretical study and simulation of light-addressable potentiometric sensors. *Phys. Status Solidi A* 211:1467–72
69. George M, Parak WJ, Gerhardt I, Moritz W, Kaesen F, et al. 2000. Investigation of the spatial resolution of the light-addressable potentiometric sensor. *Sens. Actuators A* 86:187–96
70. Itabashi A, Kosaka N, Miyamoto K, Wagner T, Schöning MJ, Yoshinobu T. 2013. High-speed chemical imaging system based on front-side-illuminated LAPS. *Sens. Actuators B* 182:315–21
71. Parak WJ, George M, Domke J, Radmacher M, Behrends JC, et al. 2000. Can the light-addressable potentiometric sensor (LAPS) detect extracellular potentials of cardiac myocytes? *IEEE Trans. Biomed. Eng.* 47:1106–13
72. Uchida H, Zhang WY, Katsube T. 1996. High-speed chemical image sensor with digital LAPS system. *Sens. Actuators B* 34:446–49
73. Das A, Chen TC, Yang CM, Lai CS. 2014. A high-speed, flexible-scanning chemical imaging system using a light-addressable potentiometric sensor integrated with an analog micromirror. *Sens. Actuators B* 198:225–32
74. Miyamoto K, Itabashi A, Wagner T, Schöning MJ, Yoshinobu T. 2014. High-speed chemical imaging inside a microfluidic channel. *Sens. Actuators B* 194:521–27
75. Wagner T, Werner C, Miyamoto K, Schöning MJ, Yoshinobu T. 2011. A high-density multi-point LAPS set-up using a VCSEL array and FPGA control. *Sens. Actuators B* 154:124–28
76. Miyamoto K, Kaneko K, Matsuo A, Wagner T, Kanoh S, et al. 2012. Miniaturized chemical imaging sensor system using an OLED display panel. *Sens. Actuators B* 170:82–87
77. Wagner T, Werner CF, Miyamoto K, Schöning MJ, Yoshinobu T. 2012. Development and characterisation of a compact light-addressable potentiometric sensor (LAPS) based on the digital light processing (DLP) technology for flexible chemical imaging. *Sens. Actuators B* 170:34–39
78. Das A, Lin YH, Lai CS. 2014. Miniaturized amorphous-silicon based chemical imaging sensor system using a mini-projector as a simplified light-addressable scanning source. *Sens. Actuators B* 190:664–72
79. Werner CF, Schusser S, Spelthahn H, Wagner T, Yoshinobu T, Schöning MJ. 2011. Field-programmable gate array based controller for multi spot light-addressable potentiometric sensors with integrated signal correction mode. *Electrochim. Acta* 56:9656–60
80. Bousse L, Mostarshed S, Hafeman D, Sartore M, Adami M, Nicolini C. 1994. Investigation of carrier transport through silicon wafers by photocurrent measurements. *J. Appl. Phys.* 75:4000–8
81. Massobrio G, Martinoia S, Grattarola M. 1992. Light-addressable chemical sensors: modelling and computer simulations. *Sens. Actuators B* 7:484–87
82. Sartore M, Adami M, Nicolini C. 1992. Computer simulation and optimization of a light addressable potentiometric sensor. *Biosens. Bioelectron.* 7:57–64
83. Parak WJ, Hofmann UG, Gaub HE, Owicki JC. 1997. Lateral resolution of light-addressable potentiometric sensors: an experimental and theoretical investigation. *Sens. Actuators A* 63:47–57
84. Guo Y, Miyamoto K, Wagner T, Schöning MJ, Yoshinobu T. 2014. Device simulation of the light-addressable potentiometric sensor for the investigation of the spatial resolution. *Sens. Actuators B* 204:659–65
85. Poghossian A, Werner CF, Buniatyan VV, Wagner T, Miyamoto K, Yoshinobu T, Schöning MJ. 2017. Towards addressability of light-addressable potentiometric sensors: shunting effect of non-illuminated region and cross-talk. *Sens. Actuators B* 244:1071–79
86. Colalongo L, Verzellesi G, Passeri D, Lui A, Ciampolini P, Rudan MV. 1997. Modeling of light-addressable potentiometric sensors. *IEEE Trans. Electron Devices* 44:2083–90

66. Provides a clear picture of the physical processes in LAPS.

68. A numerical simulation of LAPS operation by a device simulator.

74. Describes a movie recording at 100 frames per second in a microfluidic device.

87. Bandiziol A, Palestri P, Pittino F, Esseni D, Selmi L. 2015. A TCAD-based methodology to model the site-binding charge at ISFET/electrolyte interfaces. *IEEE Trans. Electron Devices* 62:3379–86
88. Bousse LJ, Parce JW, Owicki JC, Kercso KM. 1990. Silicon micromachining in the fabrication of biosensors using living cells. *IEEE 4th Tech. Dig. Solid-State Sens. Actuator Workshop* (1990):173–76
89. Miyamoto K, Sakakita S, Yoshinobu T. 2016. A novel data acquisition method for visualization of large pH changes by chemical imaging sensor. *ISIJ Int.* 56:492–94
90. Yoshinobu T, Ecken H, Poghossian A, Simonis A, Iwasaki H, et al. 2001. Constant-current-mode LAPS (CLAPS) for the detection of penicillin. *Electroanalysis* 13:733–36
91. Miyamoto K, Wagner T, Yoshinobu T, Kanoh S, Schöning MJ. 2011. Phase-mode LAPS and its application to chemical imaging. *Sens. Actuators B* 154:28–32
92. Kinameri K, Munakata C, Mayama K. 1988. A scanning photon microscope for non-destructive observations of crystal defect and interface trap distributions in silicon wafers. *J. Phys. E* 21:91–97
93. Ermolenko Y, Yoshinobu T, Mourzina Y, Levichev S, Furuichi K, et al. 2002. Photocurable membranes for ion-selective light-addressable potentiometric sensor. *Sens. Actuators B* 85:79–85
94. Hu W, Cai H, Fu J, Wang P, Yang G. 2008. Line-scanning LAPS array for measurement of heavy metal ions with micro-lens array based on MEMS. *Sens. Actuators B* 129:397–403
95. Kloock JP, Moreno L, Bratov A, Huachupoma S, Xu J, et al. 2006. PLD-prepared cadmium sensors based on chalcogenide glasses—ISFET, LAPS and ISE semiconductor structures. *Sens. Actuators B* 118:149–55
96. Mourzina Y, Yoshinobu T, Schubert J, Lüth H, Iwasaki H, Schöning MJ. 2001. Ion-selective light-addressable potentiometric sensor (LAPS) with chalcogenide thin film prepared by pulsed laser deposition. *Sens. Actuators B* 80:136–40
97. Ismail ABM, Furuichi K, Yoshinobu T, Iwasaki H. 2002. Light-addressable potentiometric fluoride (F^-) sensor. *Sens. Actuators B* 86:94–97
98. Mourzina YG, Ermolenko YE, Yoshinobu T, Vlasov Y, Iwasaki H, Schöning MJ. 2003. Anion-selective light-addressable potentiometric sensors (LAPS) for the determination of nitrate and sulphate ions. *Sens. Actuators B* 91:32–38
99. Wang JC, Ye YR, Lin YH. 2015. Light-addressable potentiometric sensor with nitrogen-incorporated ceramic Sm_2O_3 membrane for chloride ions detection. *J. Am. Ceram. Soc.* 98:443–47
100. Adami M, Piras L, Lanzi M, Fanigliulo A, Vakula S, Nicolini C. 1994. Monitoring of enzymatic activity and quantitative measurements of substrates by means of a newly designed silicon-based potentiometric sensor. *Sens. Actuators B* 18:178–82
101. Seki A, Ikeda S, Kubo I, Karube I. 1998. Biosensors based on light-addressable potentiometric sensors for urea, penicillin and glucose. *Anal. Chim. Acta* 373:9–13
102. Mourzina IG, Yoshinobu T, Ermolenko YE, Vlasov YG, Schöning MJ, Iwasaki H. 2004. Immobilization of urease and cholinesterase on the surface of semiconductor transducer for the development of light-addressable potentiometric sensors. *Microchim. Acta* 144:41–50
103. Miyamoto K, Yoshida M, Sakai T, Matsuzaka A, Wagner T, et al. 2011. Differential setup of light-addressable potentiometric sensor with an enzyme reactor in a flow channel. *Jpn. J. Appl. Phys.* 50:04DL08
104. Siqueira JR, Maki RM, Paulovich FV, Werner CF, Poghossian A, et al. 2010. Use of information visualization methods eliminating cross talk in multiple sensing units investigated for a light-addressable potentiometric sensor. *Anal. Chem.* 82:61–65
105. Fedosseeva OV, Uchida H, Katsube T, Ishimaru Y, Iida T. 2000. Novel type cholinesterase sensor based on SPV measurement technique. *Sens. Actuators B* 65:55–57
106. Werner CF, Takenaga S, Taki H, Sawada K, Schöning MJ. 2013. Comparison of label-free ACh-imaging sensors based on CCD and LAPS. *Sens. Actuators B* 177:745–52
107. Lee WE, Thompson HG, Hall JG, Bader DE. 2000. Rapid detection and identification of biological and chemical agents by immunoassay, gene probe assay and enzyme inhibition using a silicon-based biosensor. *Biosens. Bioelectron.* 14:765–804
108. Wu C, Du L, Zou L, Zhao L, Wang P. 2012. An ATP sensitive light addressable biosensor for extracellular monitoring of single taste receptor cell. *Biomed. Microdevices* 14:1047–53
109. Jia Y, Yin XB, Zhang J, Zhou S, Song M, Xing KL. 2012. Graphene oxide modified light addressable potentiometric sensor and its application for ssDNA monitoring. *Analyst* 137:5866–73

110. Wu C, Bronder T, Poghossian A, Werner CF, Bäcker M, Schöning MJ. 2014. Label-free electrical detection of DNA with a multi-spot LAPS: first step towards light-addressable DNA chip. *Phys. Status Solidi A* 211:1423–28
111. Wu C, Bronder T, Poghossian A, Werner CF, Schöning MJ. 2015. Label-free detection of DNA using a light-addressable potentiometric sensor modified with a positively charged polyelectrolyte layer. *Nanoscale* 7:6143–50
112. Wu C, Poghossian A, Bronder TS, Schöning MJ. 2016. Sensing of double-stranded DNA molecules by their intrinsic molecular charge using the light-addressable potentiometric sensor. *Sens. Actuators B* 229:506–12
113. Miyamoto K, Sugawara Y, Kanoh S, Yoshinobu T, Wagner T, Schöning MJ. 2010. Image correction method for the chemical imaging sensor. *Sens. Actuators B* 144:344–48
114. Nakao M. 2000. Visualization of defects in Si wafer using scanning laser-beam chemical microscope. *Oyo Butsuri* 69:1108–9
115. Ito Y. 1998. High-spatial resolution LAPS. *Sens. Actuators B* 52:107–11
116. Moritz W, Gerhardt I, Roden D, Xu M, Krause S. 2000. Photocurrent measurements for laterally resolved interface characterization. *Fresenius J. Anal. Chem.* 367:329–33
117. Das A, Das A, Chang LB, Lai CS, Lin RM, et al. 2013. GaN thin film based light addressable potentiometric sensor for pH sensing application. *Appl. Phys. Express* 6:036601
118. Xu C, Denk W. 1999. Comparison of one- and two-photon optical beam-induced current imaging. *J. Appl. Phys.* 85:2226–31
119. Guo Y, Seki K, Miyamoto K, Wagner T, Schöning MJ, Yoshinobu T. 2014. Novel photoexcitation method for light-addressable potentiometric sensor with higher spatial resolution. *Appl. Phys. Express* 7:067301
120. Miyamoto K, Seki K, Guo Y, Wagner T, Schöning MJ, Yoshinobu T. 2014. Enhancement of the spatial resolution of the chemical imaging sensor by a hybrid fiber-optic illumination. *Proc. Eng.* 87:612–15
121. Werner CF, Miyamoto K, Wagner T, Schöning MJ, Yoshinobu T. 2017. Lateral resolution enhancement of pulse-driven light-addressable potentiometric sensor. *Sens. Actuators B* 248:961–65
122. Nakao M, Inoue S, Oishi R, Yoshinobu T, Iwasaki H. 1995. Observation of microorganism colonies using a scanning-laser-beam pH-sensing microscope. *J. Ferment. Bioeng.* 79:163–66
123. Miyamoto K, Yu B, Isoda H, Wagner T, Schöning MJ, Yoshinobu T. 2016. Visualization of the recovery process of defects in a cultured cell layer by chemical imaging sensor. *Sens. Actuators B* 236:965–69
124. Miyamoto K, Sakakita S, Wagner T, Schöning MJ, Yoshinobu T. 2015. Application of chemical imaging sensor to in-situ pH imaging in the vicinity of a corroding metal surface. *Electrochim. Acta* 183:137–42
125. Zhang Q, Wang P, Parak WJ, George M, Zhang G. 2001. A novel design of multi-light LAPS based on digital compensation of frequency domain. *Sens. Actuators B* 73:152–56
126. Wagner T, Molina R, Yoshinobu T, Kloock JP, Biselli M, et al. 2007. Handheld multi-channel LAPS device as a transducer platform for possible biological and chemical multi-sensor applications. *Electrochim. Acta* 53:305–11
127. Miyamoto K, Kuwabara Y, Kanoh S, Yoshinobu T, Wagner T, Schöning MJ. 2009. Chemical image scanner based on FDM-LAPS. *Sens. Actuators B* 137:533–38
128. Fanigliulo A, Accossato P, Adami M, Lanzi M, Martinoia S, et al. 1996. Comparison between a LAPS and an FET-based sensor for cell-metabolism detection. *Sens. Actuators B* 32:41–48
129. Hafner F. 2000. Cytosensor® microphysiometer: technology and recent applications. *Biosens. Bioelectron.* 15:149–58
130. Stein B, George M, Gaub HE, Behrends JC, Parak WJ. 2003. Spatially resolved monitoring of cellular metabolic activity with a semiconductor-based biosensor. *Biosens. Bioelectron.* 18:31–41
131. Yotter RA, Wilson DM. 2004. Sensor technologies for monitoring metabolic activity in single cells—part II: nonoptical methods and applications. *IEEE Sens. J.* 4:412–29
132. Eklund SE, Snider RM, Wikswo J, Baudenbacher F, Prokop A, Cliffel DE. 2006. Multianalyte microphysiometry as a tool in metabolomics and systems biology. *J. Electroanal. Chem.* 587:333–39
133. Werner CF, Krumbe C, Schumacher K, Groebel S, Spelthahn H, et al. 2011. Determination of the extracellular acidification of *Escherichia coli* by a light-addressable potentiometric sensor. *Phys. Status Solidi A* 208:1340–44

113. Presents the calibration of an image to correct for the nonuniformity of current and potential.

125. A multilight LAPS was proposed for parallel readout from a plurality of pixels.

134. Yu H, Liu Q, Wang P. 2010. Light addressable potentiometric sensor (LAPS) as cell-based biosensors. In *Cell-Based Biosensors: Principles and Applications*, ed. P Wang, Q Liu, pp. 119–49. Norwood, MA: Artech House
135. Tanaka H, Yoshinobu T, Iwasaki H. 1999. Application of the chemical imaging sensor to electrophysiological measurement of a neural cell. *Sens. Actuators B* 59:21–25
136. Ismail ABM, Yoshinobu T, Iwasaki H, Sugihara H, Yukimasa T, et al. 2003. Investigation on light-addressable potentiometric sensor as a possible cell-semiconductor hybrid. *Biosens. Bioelectron.* 18:1509–14
137. Stein B, George M, Gaub HE, Parak WJ. 2004. Extracellular measurements of averaged ionic currents with the light-addressable potentiometric sensor (LAPS). *Sens. Actuators B* 98:299–304
138. Guo Y. 2017. *Development of thermally drawn multifunctional fibers and integration with field-effect sensors for biointerfaces*. PhD Thesis, Tohoku Univ., Sendai, Jpn.
139. Kohno Y, Matsuki R, Nomura S, Mitsunari K, Nakao M. 2001. Neutralization of acid droplets on plant leaf surfaces. *Water Air Soil Pollut.* 130:977–82
140. Nikaido T, Moriya K, Hiraishi N, Ikeda M, Kitasako Y, et al. 2004. Surface analysis of dentinal caries in primary teeth using a pH-imaging microscope. *Dent. Mater. J.* 23:628–32
141. Miyamoto K, Ichimura H, Wagner T, Schöning MJ, Yoshinobu T. 2013. Chemical imaging of the concentration profile of ion diffusion in a microfluidic channel. *Sens. Actuators B* 189:240–45
142. Engström O, Carlsson A. 1983. Scanned light-pulse technique for the investigation of insulator-semiconductor interfaces. *J. Appl. Phys.* 54:5245–51
143. Lundström I, Erlandsson R, Frykman U, Hedborg E, Spetz A, et al. 1993. Artificial 'olfactory' images from a chemical sensor using a light-pulse technique. *Nature* 352:47–50
144. Pecora A, Fortunato G, Carluccio R, Sacco S. 1993. Hydrogenated amorphous silicon based light-addressable potentiometric sensor (LAPS) for hydrogen detection. *J. Non-Cryst. Solids* 164–66:793–96
145. Sato T, Shimizu M, Uchida H, Katsube T. 1994. Light-addressable suspended-gate gas sensor. *Sens. Actuators B* 20:213–16
146. Zhang Q, Wang P, Li J, Gao X. 2000. Diagnosis of diabetes by image detection of breath using gas-sensitive LAPS. *Biosens. Bioelectron.* 15:249–56
147. Krause S, Talabani H, Xu M, Moritz W, Griffiths J. 2002. Scanning photo-induced impedance microscopy—an impedance based imaging technique. *Electrochim. Acta* 47:2143–48
148. Wang J, Campos I, Wu F, Zhu J, Sukhorukov GB, et al. 2016. The effect of gold nanoparticles on the impedance of microcapsules visualized by scanning photo-induced impedance microscopy. *Electrochim. Acta* 208:39–46
149. Suzurikawa J, Nakao M, Kanzaki R, Takahashi H. 2010. Microscale pH gradient generation by electrolysis on a light-addressable planar electrode. *Sens. Actuators B* 149:205–11
150. Choudhury MH, Ciampi S, Yang Y, Tavallaie R, Zhu Y, et al. 2015. Connecting electrodes with light: one wire, many electrodes. *Chem. Sci.* 6:3769–76

TABLE OF CONTENTS FOR VOLUME 1:

Annual Review of
Analytical Chemistry

Volume 10, 2017

Contents